REPORT DOCUMENTATION PAGE

Form Approved
OMB No. 0704-0188

The public reporting burden for this collection of information is estimated to average 1 hour per response, including the time for reviewing instructions, searching existing data sources, gathering and maintaining the data needed, and completing and reviewing the collection of information. Send comments regarding this burden estimate or any other aspect of this collection of information, including suggestions for reducing the burden, to the Department of Defense, Executive Services and Communications Directorate (0704-0188). Respondents should be aware that notwithstanding any other provision of law, no person shall be subject to any penalty for failing to comply with a collection of information if it does not display a currently valid OMB control number.
PLEASE DO NOT RETURN YOUR FORM TO THE ABOVE ORGANIZATION.

1. REPORT DATE *(DD-MM-YYYY)*	2. REPORT TYPE	3. DATES COVERED *(From - To)*
16-08-2012	Final	01-03-2008 - 28-02-2012

4. TITLE AND SUBTITLE

PLANT-MIMETIC HEAT PIPES FOR OPERATION WITH LARGE INERTIAL AND GRAVITATIONAL STRESSES

5a. CONTRACT NUMBER

5b. GRANT NUMBER
FA9550-09-1-0188

5c. PROGRAM ELEMENT NUMBER

6. AUTHOR(S)

Abraham Stroock - Cornell University
N. Michelle Holbrook - Harvard University
Maciej Zwieniecki - Harvard University

5d. PROJECT NUMBER

5e. TASK NUMBER

5f. WORK UNIT NUMBER

7. PERFORMING ORGANIZATION NAME(S) AND ADDRESS(ES)

Cornell University, Office of Sponsored Programs
373 Pine Tree Rd,
Ithaca, NY 14853

8. PERFORMING ORGANIZATION REPORT NUMBER

9. SPONSORING/MONITORING AGENCY NAME(S) AND ADDRESS(ES)

AFOSR
875 N RANDOLPH ST
ARLINGTON, VA 22203
Dr. Byung Lee/RSA

10. SPONSOR/MONITOR'S ACRONYM(S)

11. SPONSOR/MONITOR'S REPORT NUMBER(S)
AFRL-OSR-VA-TR-2012-1148

12. DISTRIBUTION/AVAILABILITY STATEMENT

DISTRIBUTION A: APPROVED FOR PUBLIC RELEASE

13. SUPPLEMENTARY NOTES

14. ABSTRACT

1) Design and model: we have proposed a new wick design for the operation of a heat pipe with negative pressure in the liquid path and sub-saturation everywhere in the vapor path.5 We have further developed a model of a loop heat pipe that accounts, for the first time, for tension in the liquid path; with this model, we have developed design rules for negative pressure loop heat pipes.6
2) Membranes: we have developed the first inorganic membranes capable of mediating the metastable equilibrium between liquid water and its sub-saturated vapor. Both membranes provide complete stability out to 100 bars of tension.
3) Physiology of passive robustness to cavitation in plants: in synthetic structures that mimic the segmented structure of xylem, we have demonstrated isolation of cavitation events while maintaining conductivity and characterized the coupled dynamics of cavitation.
4) Integration: we have created a functional tensiometer based on the integration of the membrane with a MEMS-based pressure sen

15. SUBJECT TERMS

heat transfer, biomimicry, microfluidics, plant science

16. SECURITY CLASSIFICATION OF:			17. LIMITATION OF ABSTRACT	18. NUMBER OF PAGES	19a. NAME OF RESPONSIBLE PERSON
a. REPORT	b. ABSTRACT	c. THIS PAGE			
U	U	U	U		19b. TELEPHONE NUMBER *(Include area code)*

Reset

Standard Form 298 (Rev. 8/98)
Prescribed by ANSI Std. Z39.18

INSTRUCTIONS FOR COMPLETING SF 298

1. REPORT DATE. Full publication date, including day, month, if available. Must cite at least the year and be Year 2000 compliant, e.g. 30-06-1998; xx-06-1998; xx-xx-1998.

2. REPORT TYPE. State the type of report, such as final, technical, interim, memorandum, master's thesis, progress, quarterly, research, special, group study, etc.

3. DATES COVERED. Indicate the time during which the work was performed and the report was written, e.g., Jun 1997 - Jun 1998; 1-10 Jun 1996; May - Nov 1998; Nov 1998.

4. TITLE. Enter title and subtitle with volume number and part number, if applicable. On classified documents, enter the title classification in parentheses.

5a. CONTRACT NUMBER. Enter all contract numbers as they appear in the report, e.g. F33615-86-C-5169.

5b. GRANT NUMBER. Enter all grant numbers as they appear in the report, e.g. AFOSR-82-1234.

5c. PROGRAM ELEMENT NUMBER. Enter all program element numbers as they appear in the report, e.g. 61101A.

5d. PROJECT NUMBER. Enter all project numbers as they appear in the report, e.g. 1F665702D1257; ILIR.

5e. TASK NUMBER. Enter all task numbers as they appear in the report, e.g. 05; RF0330201; T4112.

5f. WORK UNIT NUMBER. Enter all work unit numbers as they appear in the report, e.g. 001; AFAPL30480105.

6. AUTHOR(S). Enter name(s) of person(s) responsible for writing the report, performing the research, or credited with the content of the report. The form of entry is the last name, first name, middle initial, and additional qualifiers separated by commas, e.g. Smith, Richard, J, Jr.

7. PERFORMING ORGANIZATION NAME(S) AND ADDRESS(ES). Self-explanatory.

8. PERFORMING ORGANIZATION REPORT NUMBER. Enter all unique alphanumeric report numbers assigned by the performing organization, e.g. BRL-1234; AFWL-TR-85-4017-Vol-21-PT-2.

9. SPONSORING/MONITORING AGENCY NAME(S) AND ADDRESS(ES). Enter the name and address of the organization(s) financially responsible for and monitoring the work.

10. SPONSOR/MONITOR'S ACRONYM(S). Enter, if available, e.g. BRL, ARDEC, NADC.

11. SPONSOR/MONITOR'S REPORT NUMBER(S). Enter report number as assigned by the sponsoring/ monitoring agency, if available, e.g. BRL-TR-829; -215.

12. DISTRIBUTION/AVAILABILITY STATEMENT. Use agency-mandated availability statements to indicate the public availability or distribution limitations of the report. If additional limitations/ restrictions or special markings are indicated, follow agency authorization procedures, e.g. RD/FRD, PROPIN, ITAR, etc. Include copyright information.

13. SUPPLEMENTARY NOTES. Enter information not included elsewhere such as: prepared in cooperation with; translation of; report supersedes; old edition number, etc.

14. ABSTRACT. A brief (approximately 200 words) factual summary of the most significant information.

15. SUBJECT TERMS. Key words or phrases identifying major concepts in the report.

16. SECURITY CLASSIFICATION. Enter security classification in accordance with security classification regulations, e.g. U, C, S, etc. If this form contains classified information, stamp classification level on the top and bottom of this page.

17. LIMITATION OF ABSTRACT. This block must be completed to assign a distribution limitation to the abstract. Enter UU (Unclassified Unlimited) or SAR (Same as Report). An entry in this block is necessary if the abstract is to be limited.

Title: PLANT-MIMETIC HEAT PIPES FOR OPERATION WITH LARGE INERTIAL AND GRAVITATIONAL STRESSES

P.I.: Abraham Stroock, Chemical and Biomolecular Engineering, Cornell University
Co-P.I.: N. Michelle Holbrook, Organismic and Evolutionary Biology, Harvard University
Co-P.I.: Maciej Zwieniecki, The Arnold Arboretum, Harvard University

Contract #: FA9550-09-1-0188

PM: Byung Lip Lee

I. Summary:

Heat pipes and loop heat pipes have long been recognized as attractive alternatives to conventional heat exchangers, but the limit in the magnitude of the capillary pressures generated by the wicks in conventional designs has placed a severe limit on their applicability in vehicles and other large-scale applications. In this project, we aim to overcome this limitation by designing heat pipes with nano-porous wicks that support 10s of bars of capillary pressure. To this end, we are developing design concepts for heat pipes operating in this new regime, developing new fabrication strategies for hierarchically structured wicks that maximize capillary pressures while maintaining reasonable hydraulic resistances, and elucidating the strategies exploited by vascular plants to manage large capillary pressures and the associate metastability of the liquid phase.

II. Objectives:
1. Develop of design concepts and tools for heat pipes operated with large capillary pressures.
2. Develop materials and fabrication methods to incorporate molecularly porous wicks into good thermal conductors.
3. Elucidate plant physiological mechanisms of operation and repair for the manipulation of liquids at large negative pressures.
4. Develop prototypes of negative pressure loop heat pipes with operation under subsaturated conditions.

III. Summary of progress:
In this funding period, we have made progress on a number of fronts:
1) Design and model: we have proposed a new wick design for the operation of a heat pipe with negative pressure in the liquid path and sub-saturation everywhere in the vapor path.[5] We have further developed a model of a loop heat pipe that accounts, for the first time, for tension in the liquid path; with this model, we have developed design rules for negative pressure loop heat pipes.[6]
2) Membranes: we have developed the first inorganic membranes capable of mediating the metastable equilibrium between liquid water and its sub-saturated vapor. Both membranes provide complete stability out to 100 bars of tension.
3) Physiology of passive robustness to cavitation in plants: in synthetic structures that mimic the segmented structure of xylem, we have demonstrated isolation of cavitation events while maintaining conductivity and characterized the coupled dynamics of cavitation.

4) Integration: we have created a functional tensiometer based on the integration of the membrane with a MEMS-based pressure sensor. This structure represents the essential elements of our negative pressure heat pipe. Our preliminary work with this system has demonstrated the highest tension ever reported for such a device.

5) Physiology and biophysics of autonomic control flow and refilling in xylem. We have elucidated the control of flux through the network of segmented xylem elements and investigated two hypotheses for the mechanism of this control. We have also completed the first analysis of the biological response to cavitation in the transcriptome of a woody species and the first comparative analysis of the composition of sap in cavitated and non-cavitated vessels; based on these analyses, we have proposed a new mechanism for the autonomic response of plants to cavitation.

IV. Detailed report:

Objective 1: Fundamental understanding of and design concepts for heat pipes for operation at negative pressures.

Figure 1A presents a schematic model of a loop heat pipe with a wick capable of moving liquid under tension from a sub-saturated vapor in the condenser, against large hydraulic and inertial stresses along the liquid path, to the evaporator. Figure 2 presents the design of our prototype of such a NPLHP. The development of a wick that allows for the generation of capillary pressures, $\Delta P_{cap} \gg 1$ bar, opens two major opportunities for the design and operation of heat pipes: 1) operation in the presence of large accelerations (gravitational and dynamic) along the axis of long ($\gg 1$ m) heat pipes without failure due to dryout of the evaporator. 2) Operation of heat pipes in a sub-saturated regime in which the vapor is always superheated (sub-saturated) such that no condensation occurs in the vapor path where impedes the flow of both heat and mass; this characteristic requires a molecularly porous wick at both the evaporator and condenser. Exploiting these opportunities requires operation with liquids at negative pressures within a regime that, to the best of our knowledge, has never been explored either theoretically or experimentally. We have developed a comprehensive model of the steady state operation of a loop heat pipe that explicitly incorporates large capillary stresses and the possibility to operate in a fully sub-saturated (superheated) regime. In considering these new regimes, we have aimed to answer the following questions: 1) how does tension in the liquid phase due to adverse acceleration and hydraulic load impact performance? 2) How can a loop heat pipe be operated in a fully sub-saturated regime and what impact does this mode of operation have on performance? 3) What is the global effective conductivity of these designs and the limiting heat flow as a function of the environmental conditions and the properties of the working fluid?

Model: In building an analytical model of steady state operation, we proceeded in two steps: first, we developed the compete equations for the balances of heat, mass, and momentum for the liquid and vapor phases with two additional equations for the local thermodynamic equilibrium between the phases at the evaporator and the condenser. These equations are non-linear and coupled, but can be solved accurately with reasonable approximations (in particular, the neglect of sensible heat transfer). Second, we linearlized these equations for the limit of small variations in the temperature along the pipe. We showed that this linearlization is appropriate for a large range of operating conditions. We exploited this analysis to extract expressions for the contributions of the individual components of the system to the effective thermal resistance of the pipe. Here, we provide a summary of some of our important findings.[6]

Effective thermal resistances and conductances. The performance of a heat transfer system can be characterized by its effective thermal resistance, $\mathcal{R}_{\text{eff}}$ [K W^{-1}] or its effective thermal conductance, σ_{eff} [W K^{-1}], defined as follows:

$$\mathcal{R}_{\text{eff}} = \left(\sigma_{\text{eff}}\right)^{-1} = \frac{T_{evap}^{liq} - T_0}{q}, \tag{1}$$

where T_{evap}^{liq} is the steady state temperature of the liquid in the evaporator for a heat flow of q [W] and a maintained temperature in the liquid in the condenser, T_0. Based on linearization of the governing equations of the model heat pipe in Figure 1, we find the following expression for a saturated heat pipe:

$$\mathcal{R}_{\text{eff}}^{sub-sat} = \mathcal{R}_{\text{liq}} + \mathcal{R}_{\text{vap}} + \mathcal{R}_{\text{wick}}. \tag{3}$$

The total effective thermal resistance is the sum of components due to mass flow in the liquid ($\mathcal{R}_{\text{liq}}$) and vapor ($\mathcal{R}_{\text{vap}}$), thermal conduction through the wick ($\mathcal{R}_{\text{wick}}$). The liquid and vapor resistances depend on the properties of the working fluid on the saturation curve and the hydraulic resistances of the wick membranes (R_{wick} [Pa s kg^{-1}]), and the liquid and vapor conduits (R_{liq} and R_{vap} [Pa s kg^{-1}]):

$$\mathcal{R}_{\text{liq}} = \frac{\rho_{vap,0}}{\rho_{liq,0}} \frac{1}{\lambda \left.\dfrac{dp_s}{dT}\right|_{T_0}} \left(R_{liq} + 2R_{wick}\right) \text{ and } \mathcal{R}_{\text{vap}} = \frac{R_{vap}}{\lambda \left.\dfrac{dp_{sat}}{dT}\right|_{T_0}}, \tag{4}$$

where p_{sat} is the saturation partial pressure, λ [J/kg] is the heat of vaporization, ρ_{vap} and ρ_{liq} are the mass density of the vapor and the liquid on the saturation curve. The wick resistance is a simple sum of the resistances across the wicks in the evaporator and condenser:

$$\mathcal{R}_{\text{wick}} = 2\left(\frac{L_{w1}}{k_{w1}A_w} + \frac{L_{w2}}{k_{w2}A_w}\right), \tag{5}$$

where L_{w1} and L_{w2} [m] and k_{w1} and k_{w2} [W m^{-1} K^{-1}] are the thicknesses and thermal conductivities of the layers of the wick membranes and A_w [m^2] is the area of the evaporator and condenser. *The simple expressions in equation (4) have not been presented in the literature on heat pipes and provide invaluable information for the design systems capable of operating with large stresses.*

Figure 1B presents predictions based on the expressions in Eqs. 1-5 for water as a working fluid and T_0 = 298-373 K (25-100 °C) in a 10 meter-long heat pipe operating against an adverse acceleration of ten times gravity ($g_{total} = 10^2$ kg m s^{-2}). Despite considerable tension in the liquid (down to -22 bars), the contribution to the total resistance due to the liquid path is negligible over this entire range of temperatures. *The effective resistance of this 10 m-long system with extreme adverse acceleration is equivalent to that of ~3 mm path through cooper.* We have further shown that the dependence of the effective resistance on acceleration is entirely negligible. This analysis applies to other working fluids; in particular, we have treated the case of ammonia for which the effective operating temperature range is 250-320 K. *We conclude that, if a wick can be operated with up to 100 bars of tension without failure due to cavitation, heat can be transferred in extreme scenarios with small temperature gradients in a NPLHP.*

Objective 2: Develop materials and fabrication methods to incorporate molecularly porous wicks into good thermal conductors.

Figure 2 presents an overview of our approach for the formation of a wick structure for NPLHPs. The key elements of our design are: 1) appropriate membranes at the evaporator and condenser that can transfer large capillary stress to bulk liquid water in the liquid path (Figure 2B); 2) local structure along the liquid path that allows for cavitation events that do occur to be isolated and refilled (Figure 2C); and 3) pressure sensors to allow for monitoring the operational status of the pipe and the triggering of response to failure (Figure 2C).

Membranes. The membranes at the evaporator and condenser of a heat pipe must host the liquid phase in small pores to generate capillary pressure differences with respect to the vapor phase, high thermal conductivity to minimized temperature gradients and unnecessary superheat, high hydraulic conductivity to avoid unnecessary pressure gradients and further superheat, and high elastic modulus to avoid deformation due to capillary stresses. Current heat pipe technologies use membranes (typically wire meshes) at the evaporator and condenser that present the liquid phase in pores of diameter > 1 μm; these membranes have high thermal conductivity and hydraulic permeability but generate less than 1 bar of capillary pressure.[7] We previously demonstrated an organic membrane capable of large stresses (>200 bars of tension), but this material presented poor thermal conductivity, permeability, and mechanics.[8] In this program, we have the first two inorganic membranes capable of generating capillary stresses of this order of magnitude (100 bars) in silicon substrates that present favorable thermal and mechanical properties and are compatible with integration with both microfluidics and sensing. Figure 3 presents these membranes.

Figure 3A presents our first approach. We form this composite via deep reactive ion etching through a silicon wafer to form 10-20 μm-diameter pores; we then fill these pores with silica sol gel. The solgel cures into a glassy solid with sub-10 nm-diameter pores. Figure 3B presents a test of the stability of liquid water separated with such membranes from sub-saturated water vapor of controlled relative humidity. We find that these membranes can maintain the liquid at up to 100 bars of tension (-10 MPa) for indefinite periods of time (100% stability) and up to 200 bars with lower probability. The advantages of this strategy are its compatibility with relatively standard micromachining processes and their stability to large tensions. The disadvantages are the low hydraulic conductivity of the solgel at thicknesses for which it is mechanically stable and the tendency for rapid decrease of the stability limit upon cycling at tension.

In an effort to simplify the fabrication and composition of the membranes and improve their robustness with respect to cycling, we have developed an alternative approach based on anodically etched, porous silicon (Figure 2C). We have adapted this process to make it compatible with microfluidics (cavity on backside of wafer in Figure 2C). A stability test again demonstrated the generation of large tensions, with >98% stability out to 100 bars of tension and a maximum tension of over 250 bars (Figure 2D). These membranes present lower intrinsic permeability and provide a simple route to tuning the permeability via changes in the etch chemistry and current density; we are currently pursuing these opportunities. ***The stresses accessible with these new membranes are unprecedented in inorganic materials and point to the ability to build NPLHPs that transfer heat over large distances and against large adverse accelerations.*** We are in the midst of preparing two publications on these new membranes.[9,10]

Segmented xylem and isolation of cavitation events. Reliable use of metastable liquids requires provisions for the possibility of a cavitation event. Following the design and function of

4

vascular plants, we are pursuing the development of structures that isolate the vapor formed due to cavitation such that continuity is maintained along the liquid path from the evaporator to the condenser (Figure 2C). In plants, the xylem conduits are divided with nano-porous membranes separating adjacent segment; this architecture is believe to play a crucial role in both the passive and active management of cavitation. We have developed a segmented architecture that mimics that of xylem with micrometer-scale cavities coupled via nano-porous membranes formed of porous silicon (Figure 4A). As illustrated schematically in Figure 4A, the passage of vapor from a cavitated segment is stopped by the capture of the meniscus by the pores in the intervening membranes. Figure 4B demonstrates the functionality of this segmented architecture with regards to the isolation of cavitation events: isolated cavitation events occur within the array of cavities without the vapor spreading to adjacent cavities in which the liquid remains under tension (above 100 bars in this case). ***This represents the first successful mimic of the physical mechanism that is observed in plants and points to the ability to avoid catastrophic failure in technologies such as NPLHPs operating with metastable liquids.***

We have characterized the dynamics of cavitation in this unprecedented structure. Of note is that cavitation events proceed in bursts, as seen in the time-sequence of events in Figure 4C and the time autocorrelation function in Figure 4D: a group of segments cavitates every ~5 minutes; the spatial distribution of the events is random. This behavior is reminiscent of avalanche dynamics that are observed in other systems far from equilibrium. To investigate the origin of this correlation, we measured the acoustic signals emitted by these cavitation events to test the hypothesis that these cavitation events trigger one another. Figure 4E presents the ring down after a single event. While a robust ultrasonic signal is produced by each event, the characteristic time of decay of these signals is far too short (~1 ms) to explain the 5 minute period that is observed in the time correlation. ***We note that these acoustic events could be used as a means to sense the occurrence of a cavitation event and the identity of the cavitated segment such that a localized refilling process could be initiated; such a mechanism has been proposed in plants[11].*** Our second hypothesis for the origin of this time correlation is that the cavitations suppress one another: upon cavitation, liquid at the saturation vapor pressure is released into the sample, relieving the stress, and thus also the metastability, of the other cavities in the sample. Figure 4F presents a histogram of the time required for a single cavity to empty; this is the time over which liquid is released by the cavity and metastability is relieved. The fact that the average emptying time is 5 minutes is compatible with the hypothesis that the persistent time correlations are defined by the dynamics of saturation and desaturation. ***The new physics elucidated by these experiments informs the design of synthetic systems exploiting metastable liquids and may lead to a new understanding of the dynamics of transport in vascular plants.***

Objective 3: Structure and molecular biology of xylem that control stability and refilling:

Beyond the passive robustness against cavitation discussed above, experiments suggest that plants also manage flow and stresses within sap via active processes. Our team has played an active role in the elucidation of these phenomena and the development of models to explain their operation. Understanding of these autonomic processes in plants will inform design of synthetic systems capable of operating robustly with metastable liquids.

Local, autonomic control of flows within xylem networks.

As discussed above, xylem conduits form a network of interconnected segments separated by nano-porous structures called border pit membranes (BPMs); Figure 5A shows

5

individual BPMs in an SEM. Previously, Zwieniecki and Holbrook demonstrated that these membranes present variable hydraulic conductance as a function of the composition of the sap.[1] In particular, they found that conductance rises with rising ionic strength (Figure 5B) and pH. Via the localized secretion of solutes into the stream of sap, plants can use this variability of the conductance of BPMs to manipulate the spatial distribution of the flux of water and nutrients during transpiration to manage heterogeneity in resources and demand. A first challenge in defining the mechanism underlying this response is the lack of physiological data on the structure and material properties of BPMs. In this project, we have characterized the properties of BPMs with unprecedented detail.[4] Figure 5C shows AFM analysis of an individual BPM in its hydrated state at low (left) and high (right) ionic strength. Interestingly, the morphology and apparently modulus of the surface change, with larger topography and lower modulus at low salt and smaller topography and higher modulus at high salt. This observation supports the hypothesis presented in Figure 5D in which a hydrogel (e.g., pectin) coats a rigid, nano-porous scaffold (e.g., formed of cellulous fibers) in the BPMs. In this scenario, the variability of conductance could arise due to the collapse of the ionic gel with increasing ionic strength: in the collapsed state, the hydraulic diameter of the pores would be larger and the conductance would be higher.

We have also developed a second model of the flow through BPMs in an attempt to explain the variations of conductance as a function of ionic strength and pH. Studies by other investigators indicate that, depending on the species, the BPM conductance can either increase or decrease as a function of ionic strength.[12] Figure 6A presents the flow of sap through a pore with charged walls. This scenario can also lead to conductance that depends on both ionic strength as pH, as follows: net ionic charge accumulates in a screening layer adjacent to the charged walls; the thickness of this layer depends on ionic strength. In the presence of a press-driven flow, these mobile charges are convected down the channel and lead to an opposing electric field. In turn, this induced electric field drives ionic current and electroosmotic flow back along the channel, opposing the principle flow. The net effect is the so-called electro-viscous effect: the apparent hydraulic conductance is less than that in a pore with neutral walls and depends on the ionic strength and the surface charge density. Figure 6B presents the predictions of an electrokinetic model of this scenario with surface charge density taken from values measured on plant tissues. Importantly, this model predicts that, depending on the dimension of pores in the membrane and the absolute values of ionic strength used, the conductance can either increase or decrease as a function of salt concentration. Figure 6C further shows that, for chemistries that approximate that of pectin, the model captures the pH dependence that has been observed. A manuscript on this model is near submission.[13] *This electrokinetic model suggests new experiments in plants to distinguish between the two scenarios. It also provides a convenient path for the implementation of flow control in synthetic xylem via manipulation of surface charge and composition of the working fluid.*

Autonomic repair of cavitated vessel segments. When cavitation does occur locally within the xylem network, many woody species are able to refill the vessel without global relief of tension; the biological and physical mechanisms by which this process occurs have remained unclear (Figure 7A). In this project, we have acquired important new data to inform our understanding of our emerging model of this process. In a first set of experiments, we performed the first analyses of the transcriptome response (~64000 genes) to embolism in poplar (*Populus trichocarpa*) stems (Figure 7B).[3,14] It is evident that embolism is being sensed by the living cells

surrounding the xylem and that signal triggers massive (~9000 genes) and significant (p-value<0.00001) transcription responses of genes from many gene ontology (GO) groups. The origin of the signal might be related to sucrose buildup in the apoplast compartment. This hypothesis is supported by significant overlap of the transcriptome response found in stems with vessels infiltrated by sucrose to these experimentally embolized. However, transcriptome analysis also suggests presence of a different scenario in which the diffusion of air (oxygen) into the embolized vessels triggers the initial response directly via reduction of hypoxic stress and reduction in the level of reactive oxygen species. ***The question of the signal's origin is biologically very important and if understood could provide ideas for bio-inspired detection systems in microfluidic devices.***

In a complementary study, we have performed the first analysis of the composition of the sap in cavitated vessels in order to clarify the kinetics and thermodynamics of refilling.[2] Figure 7C shows: 1) that the composition of sap in cavitated vessels is substantially different than in filled ones; this observation supports the hypothesis that adjacent, living cells are providing the energy source to drive refilling by increasing the osmotic strength locally. 2) The osmotic strength in cavitated vessels reaches the magnitude required to recruit water from adjacent vessels under tension when stress is relieved but not eliminated in the recovering plant (blue circles and dotted line in right hand plot in Figure 7C).

Taken together, these new experiments provide a foundation for the most complete theory of local refilling date. Figure 8 presents the current state of our model, covering triggering, cellular processes, and local manipulation of mass and energy fluxes.[2] ***This detailed model for a local recovery process provides a template for strategies to pursue in synthetic technologies that operate with metastable liquids.***

Objective 4: Development of prototype of NPLHP:

An important challenge in the development of a full prototype of a NPLHP is the integration of the membranes discussed under Objective 1 with conventional microfabrication processes that are required for the formation of microfluidic conduits and sensing elements. In order to perfect these methods, we have focused on the integration of a diaphragm pressure sensor with a single nano-porous membrane. This structure represents half of the wick structure of a NPLHP (Figure 2A) and contains the critical components. It also represents an important technology in itself, a microtensiometer. A tensiometer allows for the chemical potential of an external phase of a fluid (e.g., water) to be measured as a pressure (or tension for a sub-saturated phase). Conventional tensiometers are macroscopic in dimension and have a very limited range of function (less than 1 bar). Our system aims at providing a dramatically larger range of function (100 bars) in a format that will allow for sensing with an unprecedented spatial resolution. We have applied for a patent on this concept.[15]

Figure 9A presents a photograph of a microtensiometer. This structure integrates a pressure sensor with an operational range that can be extended beyond 100 bars. Figure 9B shows a calibration curve and the linearity of the response of one of these sensors. We have successfully integrated this sensor with our first class of membranes formed for solgel in the pores of a through-etched silicon wafer (Figure 9C). We have successfully developed MEMS pressure sensors with which to monitor the stress in the liquid phase of our NPLHPs. This stress is a key parameter in the definition of appropriate operation and in the implementation of strategies to recover operation after cavitation. We have recently achieved calibrated measurements the liquid pressure as a function of the activity of the vapor outside the device (Figure 9D). ***With direct mechanical measurements of tension out to -30 bars, we have***

drastically increased the range over which any tensiometer has been operated; this development has important technological consequences for a variety of fields in agriculture and environmental science in which precise measurements of the chemical potential of water are crucial. These experiments also represent an important step toward realizing our goal of NPLHPs. In parallel with these efforts, we have developed a system with which to control vapor flows and activities with high precision. This system will allow us to characterize the function of our complete wick with complete control over the thermodynamic state of the fluid and of the fluxes of heat and mass.

We note that we have not addressed all of the challenges in the fabrication of these integrated devices. In particular, we still have low yields of functional pressure sensors and, even when functional, the connections to the piezo resistive elements show variable contact resistance. We have identified the process step at which these problems arise and we are implementing a solution. We must also reduce the hydraulic resistance of the membrane so that this resistance will not lead to excessive pressure drop (and cavitation) at high heat fluxes in a NPLHP. We are currently integrating the porous silicon membrane (Figure 3C) into this process to benefit from its lower resistance.

V. Future directions.

Model: We will continue the development of our model of NPLHP operation to capture time dependence. Such models will allow us to model the transients that occur upon start-up when instabilities can arise.

Components: We will continue to pursue the implementation of segmented vessels with the aim of incorporating appropriate structures in the liquid paths of NPLHPs to guard against catastrophic failure upon cavitation. We will also pursue ideas inspired by plants for refilling cavitated zones of the liquid path with local generation of pressure gradients. We have a model based on electrokinetic flows that builds on our understanding of pore-scale processes in border pit membranes (Figure 6).[13]

Biology: We will continue to pursue the details of the biological and biophysical mechanisms underlying the control of fluxes (Figure 5) and local refilling in plants (Figure 8). With regards to flow control, we will perform experiments informed by our two hypotheses (Figure 5D and Figure 6) and develop a refined theoretical model of transport through composite gel-fiber structures. With regards to refilling, we will focus on the firm identification of the signals that trigger the refilling activity and on the means by which final reconnection of liquid between the refilling segment and the adjacent segments under tension occurs.

Integration: We are now fabricating complete wicks with evaporator and condenser membranes formed of porous silicon. This year, we aim to characterize the operation of the wick (liquid path) at negative pressures with independent control of the vapor at the evaporator and condenser. We will then move to closed-loop operation in both saturated and sub-saturated regimes. We expect these experiments to provide a foundation of understanding for the design and operation of NPLHPs. Our prototype-scale system could also serve as a technological solution for small scale heat transfer problems, for example, in electronic cooling.

V. Bibliography

1. Zwieniecki, M. A., Melcher, P. J. & Holbrook, N. M. Hydrogel control of xylem hydraulic resistance in plants. *Science* **291**, 1059-1062 (2001).

2.   Secchi, F. & Zwieniecki, M. A. Analysis of xylem sap from functional (non-embolized) and non-functional (embolized) vessels of Populus nigra - chemistry of refilling. *Plant Physiology (in press)* **157**, 1419-1429 (in press 2012).

3.   Secchi, F., Gilbert, M. E. & Zwieniecki, M. A. Transcriptome response to embolism formation in stems of Populus trichocarpa provides insight into signaling and biology of refilling. Plant Physiology *Plant Cell and Environment* **157**, 1419-1429 (2011).

4.   Lee, J., Holbrook, N. M. & Zwieniecki, M. A. Ion induced changes in the structure of bordered pit membranes. *Frontiers in Plant Biophysics and Modeling* **3**, 55 (2011).

5.   Stroock, A. D. & Wheeler, T. D. High Performance Wick. USA patent PCT/US09/42832 (2009).

6.   Chen, I.-T., Pharkya, A. & Stroock, A. D. Analysis of plant-inspired heat pipe for operation under extreme conditions. *International Journal of Heat and Mass Transfer* (in submission 2012).

7.   Faghri, A. *Heat Pipe Science and Technology*. (Taylor and Francis, 1995).

8.   Wheeler, T. D. & Stroock, A. D. The transpiration of water at negative pressures in a synthetic tree. *Nature* **455**, 208-212 (2008).

9.   Chen, I.-T., Pagay, V., Sessoms, D. A., Sherman, Z. M. & Stroock, A. D. Characterization of two inorganic membranes for the maintenance of metastable liquid vapor equlibrium. (in preparation 2012).

10.   Chen, I.-T., Sherman, Z. M. & Stroock, A. D. Temperature-dependent stability limit of liquid water in metastable equilibrium with sub-saturated vapors. (in preparation 2012).

11.   Salleo, S., Trifilò, P. & Lo Gullo, M. A. Vessel wall vibrations: trigger for embolism repair? *Functional Plant Biology* **35**, 289-297 (2008).

12.   Cochard, H., Herbette, S., Hernandez, E., Holtta, T. & Mencuccini, M. The effect of sapioniccom-position on xylem vulnerability to cavitation. *Journal of Experimental Botany* **61**, 275–285 (2010).

13.   Santiago, M., Pagay, V. & Stroock, A. D. Theoretical Analysis of Electroviscous Effects on Flow through Xylem Bordered Pit Membranes. (in preparation 2012).

14.   Secchi, F. & Zwieniecki, M. A. Sensing embolism in xylem vessels: the role of sucrose as a trigger for refilling. *Plant Cell and Environment* **34**, 514-524 (2011).

15.   Stroock, A. D., Lakso, A. N., Pagay, V., Llic, B. & Metzler, M. Microtensiometer sensor, probe, and method of use. PCT/US10/31454 (2010).

16.   Aida, M. & Dupuis, M. IR and Raman intensities in vibrational spectra from direct ab initio molecular dynamics: D2O as an illustration. *Journal of Molecular Structure-Theochem* **633**, 247-255 (2003).
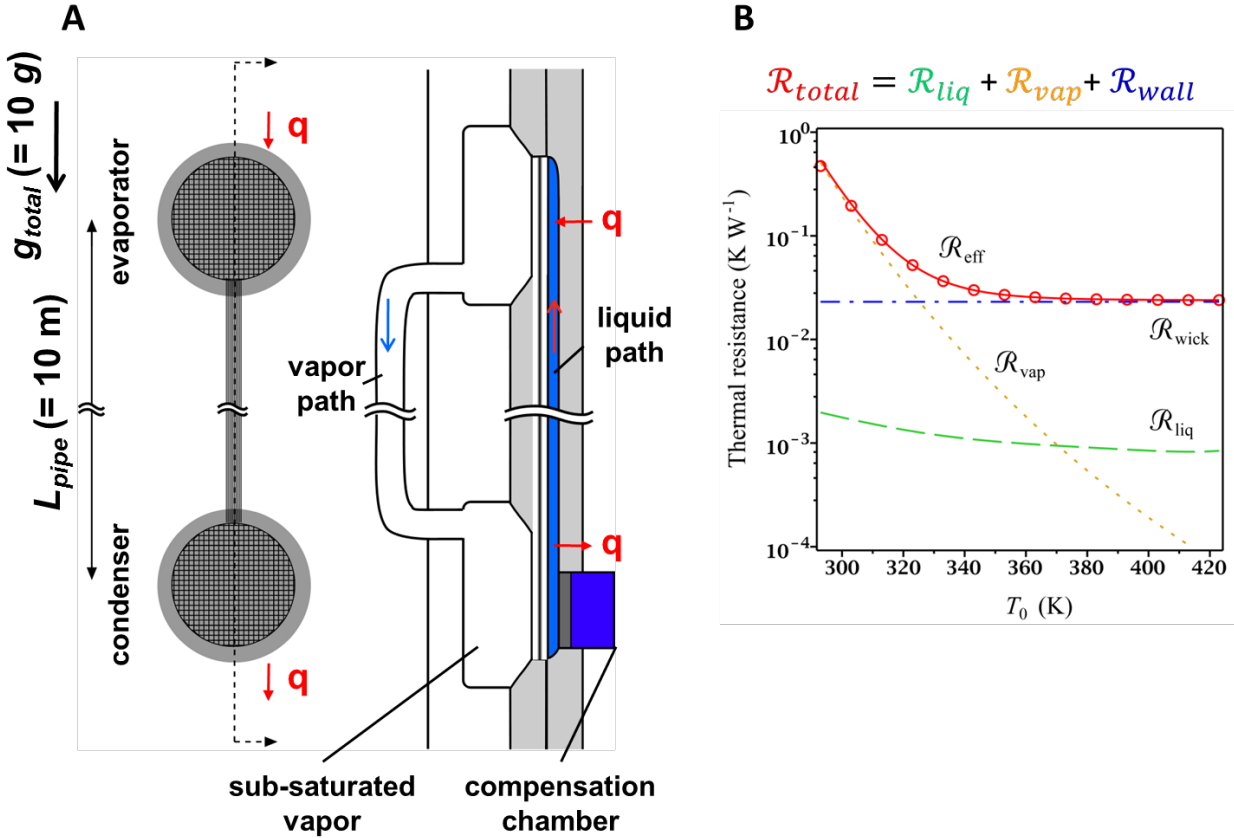
Figure 1: Model of negative pressure loop heat pipe (NPLHP). (A) Schematic representation of NPLHP showing top-view of wick (left) and cross-sectional view of wick and vapor path (right). **(B)** Predictions of effective thermal resistance of NPLHP operating at $q = 10$ W cm^{-2} with a total length, $L_{pipe} = 10$ m and total adverse acceleration $g_{total} = 10$ g $= 10^2$ kg m s^{-2}. The predictions in (B) were made with eqns. (1-5). The properties of water (liquid and vapor) on the saturation curve were taken from NIST (http://webbook.nist.gov/chemistry/fluid/). The characteristics of the heat pipe were as follows: length, $L_{pipe} = 10$ m; diameter of vapor path, area of evaporator and condenser, $A = 10^{-4}$ m^2; diameter of liquid and vapor conduits, $d_{liq} = 350 \times 10^{-6}$ m and $d_{vap} = 6 \times 10^{-3}$ m; thickness of layer 1 and layer 2 of wick, $L_1 = 2 \times 10^{-6}$ m and $L_2 = 350 \times 10^{-6}$ m; pore diameter in layer 1 and layer 2, $d_{pore1} = 5 \times 10^{-9}$ m and $d_{pore2} = 200 \times 10^{-9}$ m; pore fraction of both layers of wick, $\phi = 0.6$; thermal conductance of wick, $k_{wick} = 130$ W m^{-1} K^{-1} (silicon); acceleration along pipe, $g_{total} = 10$ m s^{-2}.

A

silicon

"leaf"   "root"

1 cm

B root/leaf membrane

silica solgel   silicon

C segmented vessels

Si

nanoporous silicon

D piezoresistive pressure sensors
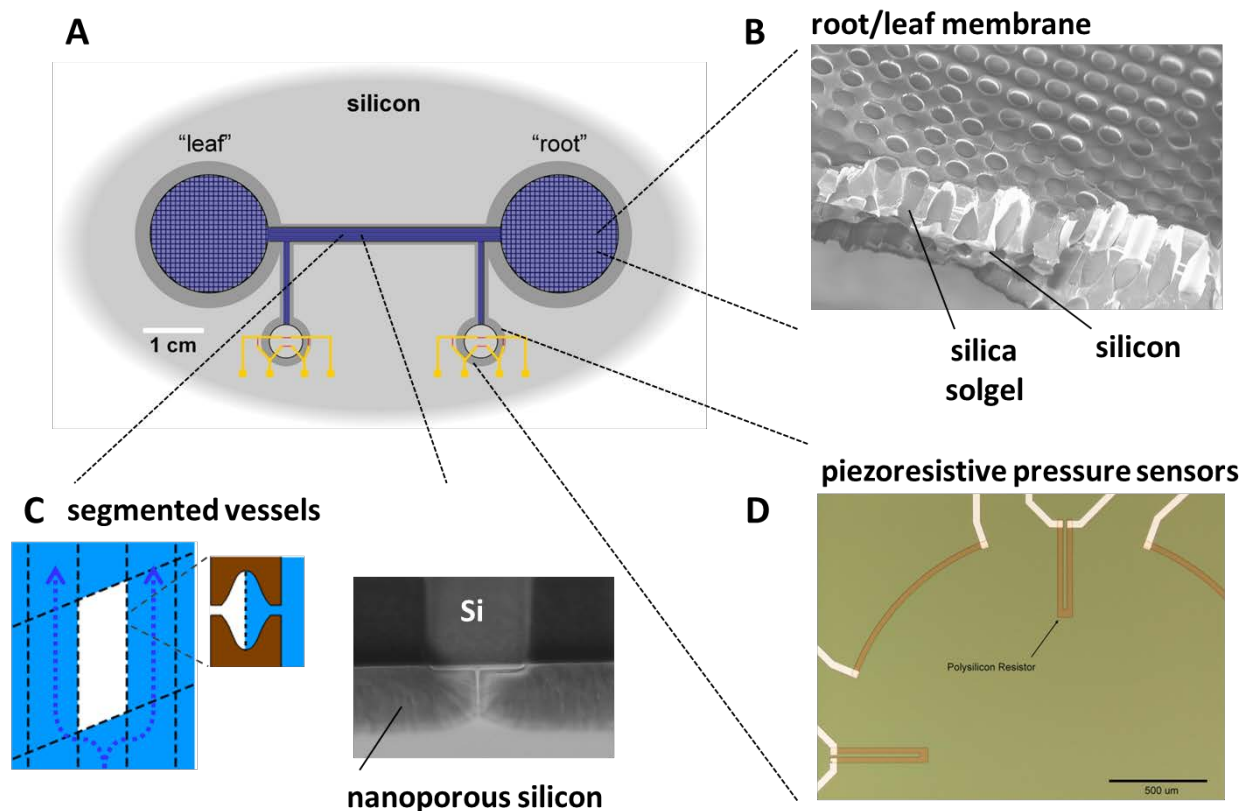
Polysilicon Resistor

500 um

Figure 2: Silicon platform for plant-inspired LHP. **(A)** Schematic diagram of wick structure with integrated pressure sensors. **(B)** Composite silicon-silica membrane. **(C)** Schematic representation of segmented xylem vessels with an isolated vapor bubble and redirected flow (left). SEM of cross-section of an anodically etched silicon wafer with a masked area on the surface (right). **(D)** Micrograph of a section of two branches of a Wheatstone bridge of poly(silicon) resistors on a silicon diaphragm.
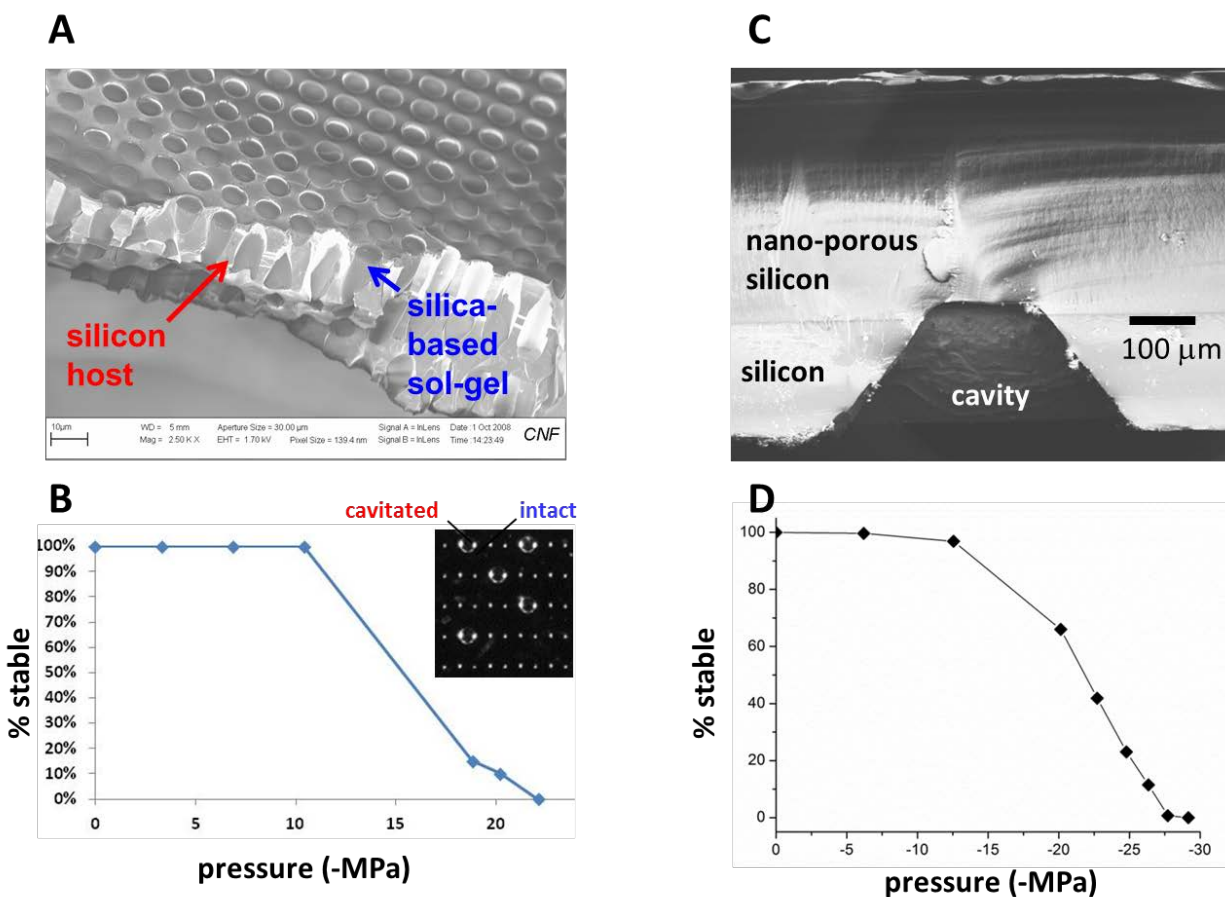
Figure 3: Development of inorganic membranes for generating large tensions. (**A**) SEM of cross-section of composite membrane with through-etched pores in silicon filled with a silica sol-gel. (**B**) Stability of liquid placed in equilibrium with sub-saturated vapors via the composite membrane in (A). Reported is the percentage of cavities (of 625) that remained stable at each tension. Inset shows an optical micrograph of 25 cavities; dark cavities are filled and bright cavities are empty (cavitated). (**C**) Optical micrograph of a silicon membrane that has been anodically etched from the top to form nano-porous silicon and wet etched from the bottom to form a cavity. (**D**) Stability of liquid placed in equilibrium with sub-saturated vapors via the composite membrane in (C). Reported is the percentage of cavities (of 625) that remained stable at each tension.
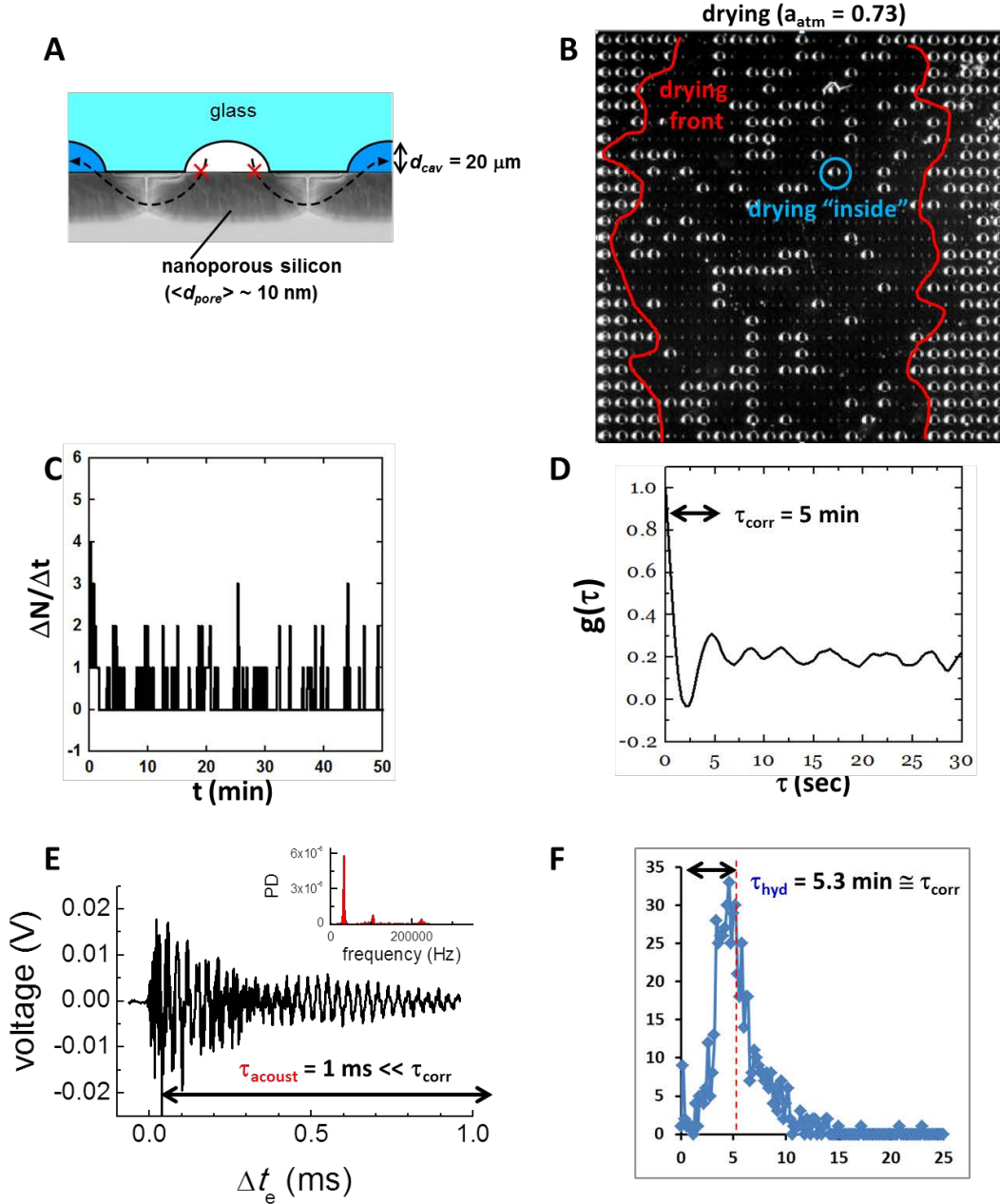
Figure 4: Segmented, artificial xylem conduits for isolation of cavitation events. (A) Schematic diagram showing cross-section of isolated cavities formed in glass bonded to a substrate with a surface layer of nano-porous silicon. (B) Optical micrograph of an array of cavities as in (A). The sample was drying into an atmosphere at 73% RH via the right and left edges. Dark cavities were full with liquid water; bright cavities were empty after cavitation. (C) Time series of cavitation events from a drying experiment as in (B). Periodic bursts of events are visible. (D) Time auto-correlation function of cavitation events from time series in (C). There is a correlation time, $\tau_{corr} = 5$ min between bursts. (E) Signal from an ultrasonic acoustic sensor from a single cavitation event in a sample as in (B). Typical ring down time, $\tau_{acoust} = 1$ ms. (F) Histogram of emptying times of individual cavities (population size = 625). Average emptying time, $\tau_{hyd} = 5.3$ min.
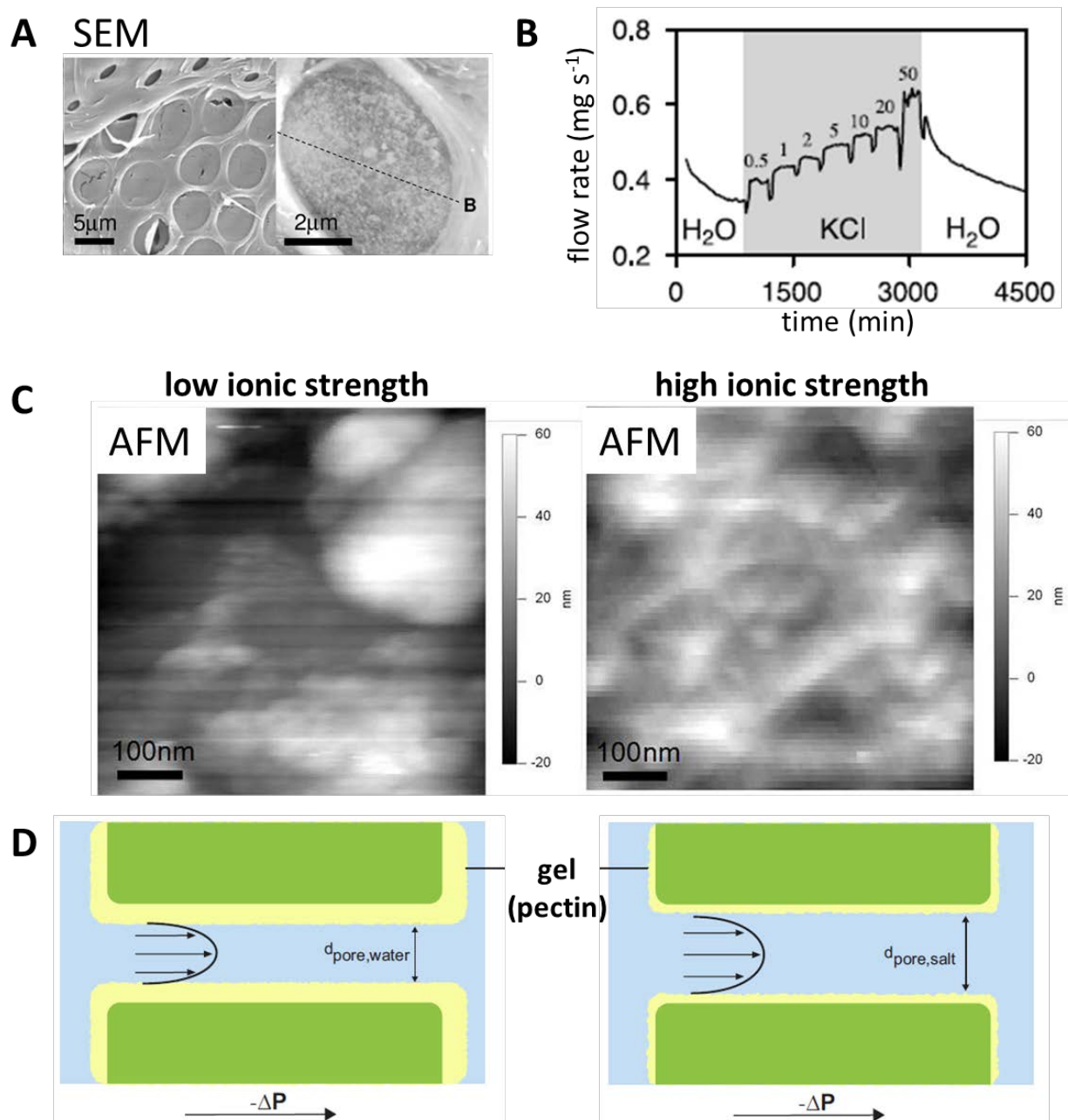
Figure 5: Autonomic control of flow within segmented xylem. **(A)** Flow through a segment of xylem in a live tobacco plant as a function of time at constant pressure difference. The ionic strength of the sap was varied with the addition of KCl.[1] **(B)** SEM of border pit membranes (dry). **(C)** AFM of individual border pit membrane at low (left) and high (right) ionic strength.[4] **(D)** Proposed mechanism by which ionic strength controls hydraulic conductance of pores through border pit membrane: a gel (e.g., pectin) coats the pores and collapses at high ionic strength.
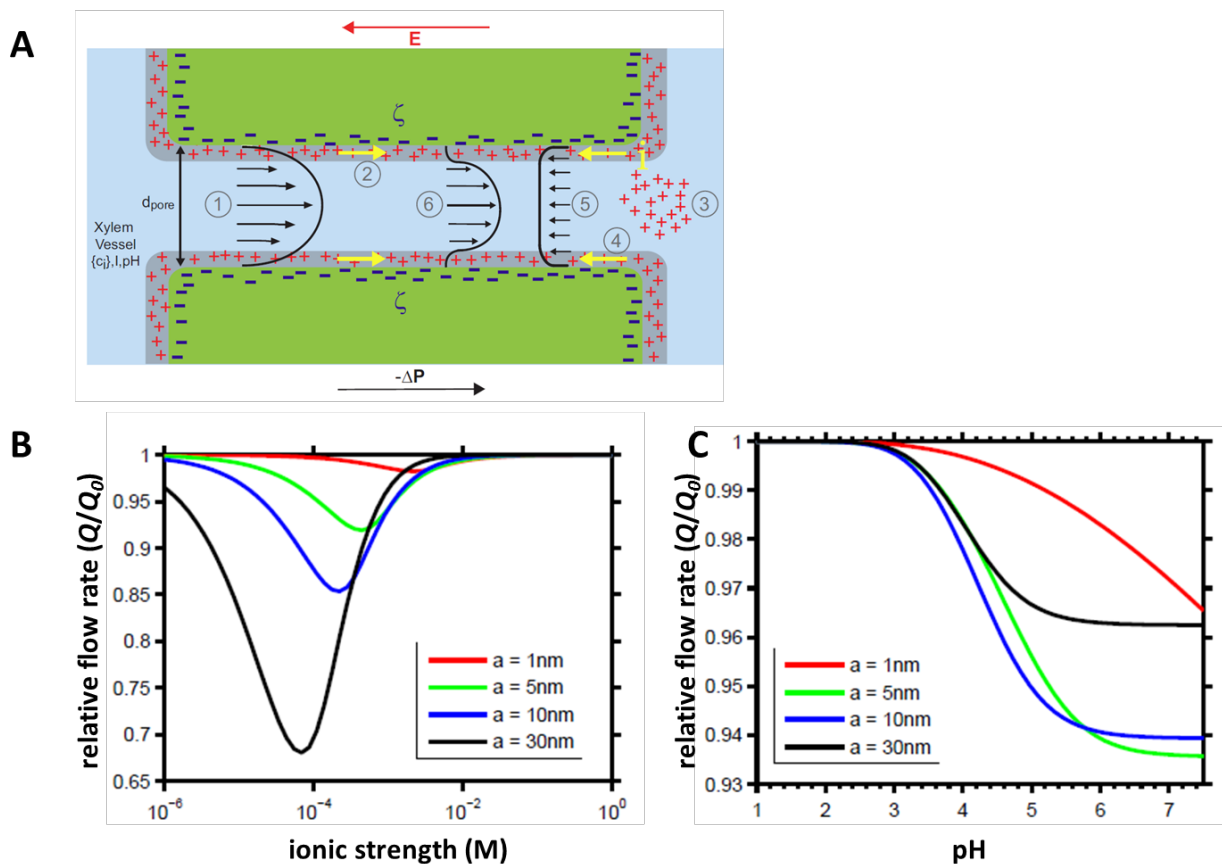
6,16

Figure 6: Electrokinetic model of autonomic control of .local flow control **(A)** Schematic diagram of pressure-driven flow (1) and electroosmotic counter flow (2) through a charged pore in through a border pit membrane. **(B)** Relative flow rate through a pore as in (A) as a function of ionic strength. The flow with charged walls, Q, is less than the flow without charged walls, Q_0. **(C)** Relative flow rate as in (B) as a function of pH.
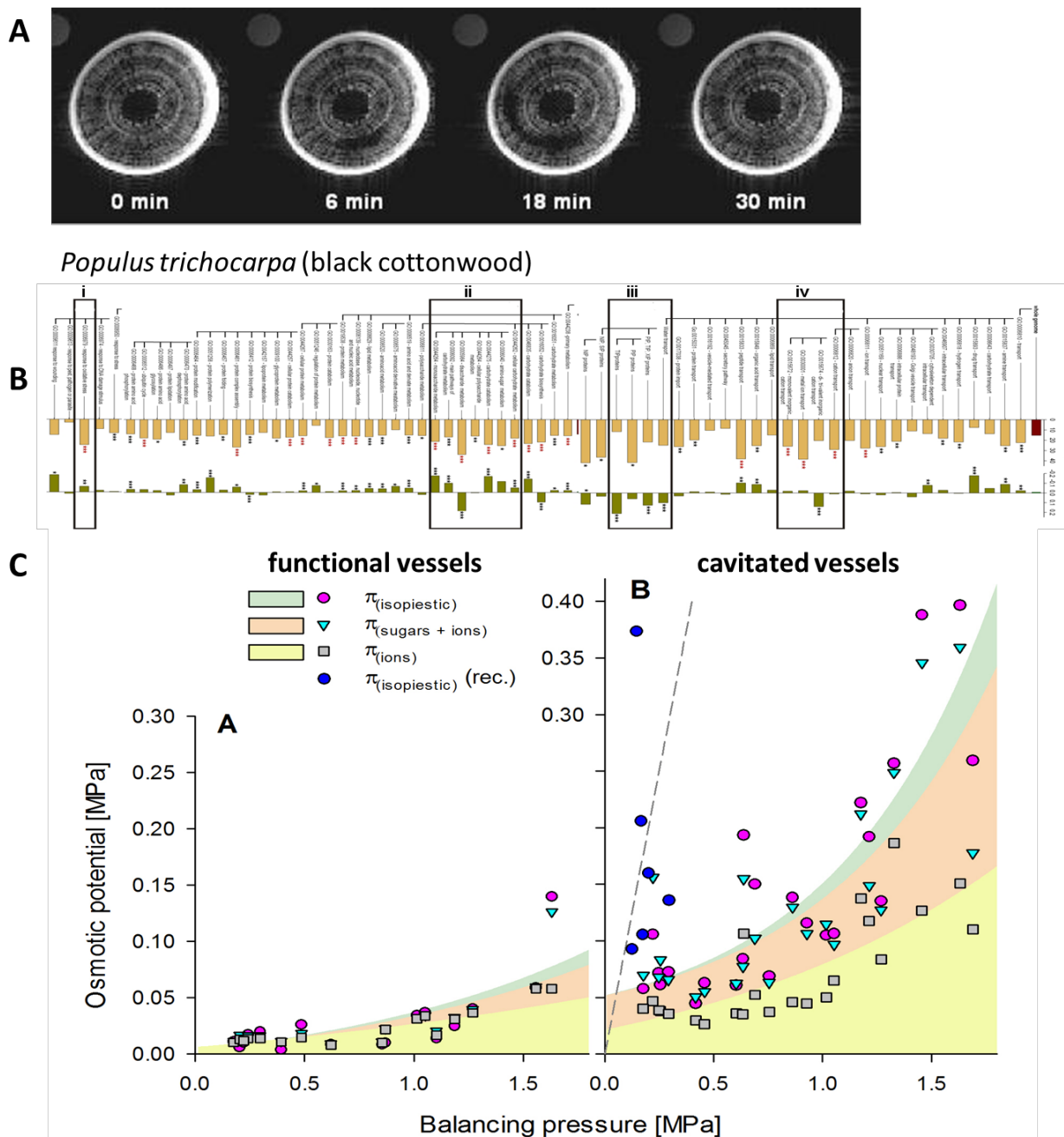
Figure 7: Autonomic repair after cavitation. (A) MRI images of cavitation event(dark zone) and repair. **(B)** Differential regulation of genes after embolization that support hypotheses in (A): **(i,ii)** changes in ion transporter and aquaporin transcription activity; **(iii)** changes in transcription of carbohydrate metabolism; and **(iv)** down regulation of genes for oxidative stress.[3] **(C)** Analysis of osmolytes in sap found in filled ("functional") and cavitated vessels.[2]
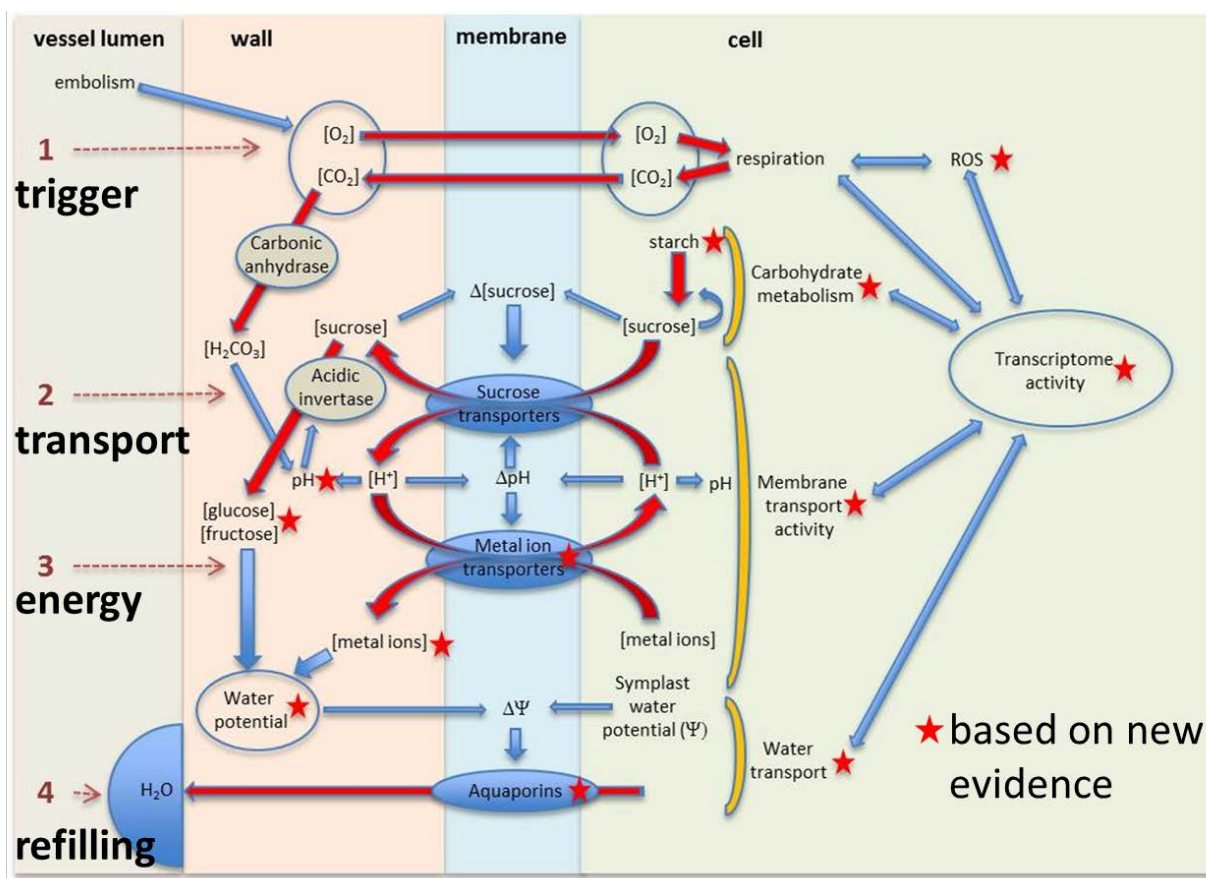
Figure 8: Biophysical model of cellular activity during refilling and gene categories response to embolism. Formation of an embolism triggers cascade of transcription-level cellular response that prepares cell for refilling activity. Changes in the gas composition and diffusion rates in the embolized vessel provides oxygen for respiration and removes CO_2 from cell vicinity and triggers transport. [2]
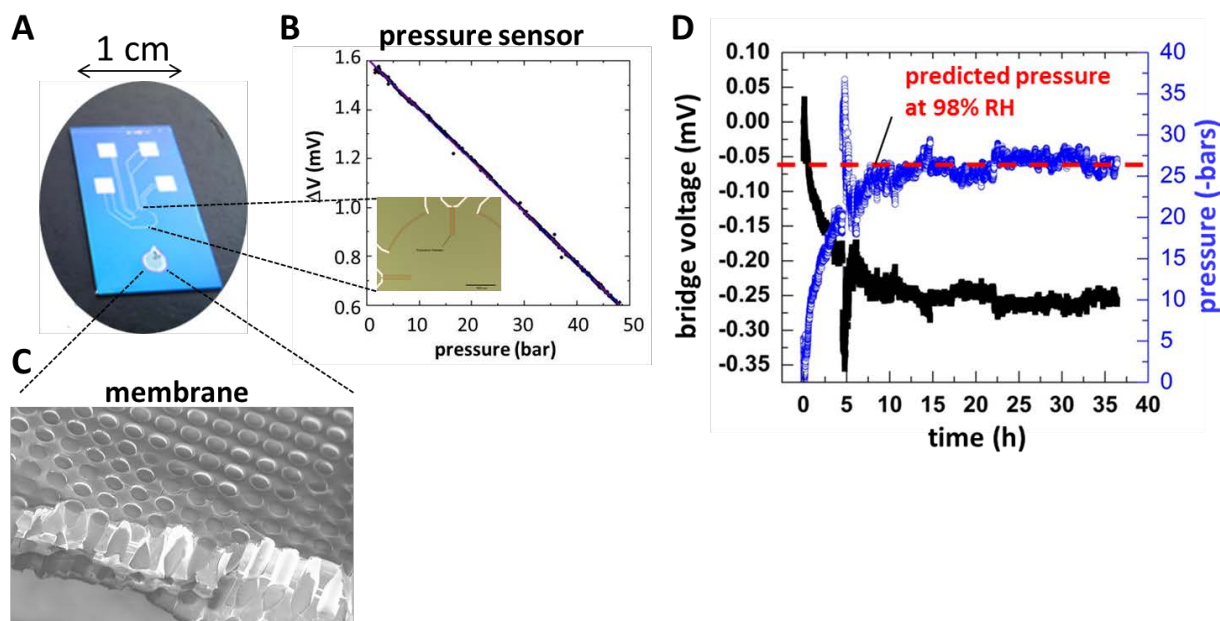
Figure 9: Integrated membrane and pressure sensor. Microtensiometer. **(A)** Photo of a microtensiometer. Four contact pads and leads to Wheatstone bridge of poly(silicon) resistors are visible at top of chip. Membrane region is visible at bottom of chip. Microfluidic channel is on back side of chip. **(B)** Integrated sensing. Plot shows voltage response of piezo-resistive diaphragm pressure senor as a function of applied pressure. Inset shows micrograph of sensor area. **(C)** Composite silicon-solgel membrane. **(D)** Response from integrated pressure sensor to an abrupt change in the vapor pressure outside the wick membrane.